Journal of Materials Chemistry C

ROYAL SOCIETY OF CHEMISTRY

PAPER

Cite this: J. Mater. Chem. C, 2023, 11, 609

2D spin glass $MnIn_2Se_4$: application of liquid-phase exfoliation to a layered structure with seven-atom-thick layers†

Govind Sasi Kumar,[a] Yan Xin,[b] J. S. Raaj Vellore Winfred,[a] Judith K. Clark[a] and Michael Shatruk *[ab]

Received 7th September 2022,
Accepted 8th December 2022

DOI: 10.1039/d2tc03776a

rsc.li/materials-c

We report liquid-phase exfoliation (LPE) of bulk layered-structure semiconductor, $MnIn_2Se_4$, to nanoscale thick sheets by ultrasonication followed by sequential centrifugation at 2000, 5000, and 7500 rpm. The nanosheets exfoliated by LPE in isopropyl alcohol show an average thickness of 50, 40, and 14 nm, respectively. The smallest of these values corresponds approximately to ten 7-atom thick [Se–In–Se–Mn–Se–In–Se] layers that compose the bulk structure of $MnIn_2Se_4$. Both the bulk material and the exfoliated samples show photoluminescence, but the weak shoulder observed from the indirect band gap emission is obviously suppressed in the nanosheet samples as compared to the bulk sample. Similar to the bulk, the nanosheets isolated at 2000 and 5000 rpm exhibit spin-glass behavior with a freezing temperature of ~3 K. In contrast, the nanosheets isolated at 7500 rpm do not exhibit any anomalies in their low-temperature magnetic behavior. These results demonstrate the possibility to extend the LPE technique to van-der-Waals materials with several-atom-thick layers.

Introduction

Over the past decade, the field of 2D materials has been one of the most rapidly developing domains in materials science.[1–4] Structure confinement to two dimensions leads to unique optical,[5] transport,[6] and magnetic properties[7] that distinguish 2D materials from their 3D layered counterparts. The promise of 2D materials for various surface-related applications, such as catalysis,[8] integrated circuits,[9] electronic devices,[10] and quantum technologies,[11] is evident in the extensive research efforts in these areas. These materials can also host a wide variety of correlated phenomena, including exotic topological states[12] and unconventional superconductivity.[13]

Similar to 2D materials in general, magnetic 2D materials offer the possibility to discover new behaviors that can be leveraged for novel applications. In this regard, a groundbreaking discovery was the observation of layer-dependent magnetism in CrI_3.[14] Bulk crystalline CrI_3 shows ferromagnetic (FM) ordering below Curie temperature (T_C) of 61 K. Monolayer CrI_3 obtained by mechanical exfoliation also showed FM ordering, but a bilayer structure showed antiferromagnetic (AFM) ordering.[14] Another layered ferromagnet, $CrGeTe_3$, showed a higher sensitivity of the T_C value to applied field when exfoliated to ultrathin flakes.[15]

Along with the extensive search for new 2D materials, including 2D magnets, there has been a consistent effort to develop alternative methods for the preparation of such materials. The traditional mechanical exfoliation, commonly known as the scotch-tape method, while clean and convenient, offers limited scalability. To expand the potential of using the unique optical, electronic, magnetic, and structural properties of 2D materials in various applications, the proper preparation and scale up of these materials is important. Chemical vapor deposition (CVD)[16] and liquid-phase exfoliation (LPE)[17,18] have emerged as two most prominent approaches for a large-scale production of 2D materials. The LPE method was pioneered by Coleman and co-workers[19] and subsequently adopted by many other groups, providing an efficient way for the preparation of such popular 2D materials as graphene,[20,21] transition metal dichalcogenides (TMDs),[22] and boron nitride (BN).[23] In particular, sonication-assisted LPE has proven effective for the synthesis of 2D nanosheets. In this process the bulk material is dispersed in a suitable solvent and subjected to ultrasonication for a long time (>5 h). The layered material is broken into nanosheets due to shock waves generated by the collapse of bubbles produced by ultra-sonication. Then, the nanosheets are separated into fraction of different thickness by

[a] Department of Chemistry and Biochemistry, Florida State University, 95 Chieftan Way, Tallahassee, FL 32306, USA. E-mail: shatruk@chem.fsu.edu
[b] National High Magnetic Field Laboratory, 1800 E Paul Dirac Dr, Tallahassee, FL 32310, USA

† Electronic supplementary information (ESI) available. See DOI: https://doi.org/10.1039/d2tc03776a

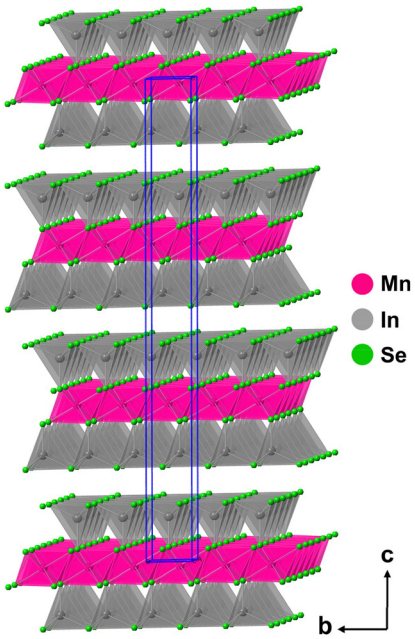

Fig. 1 The layered crystal structure of $MnIn_2Se_4$, showing the van-der-Waals gaps between 7-atom-thick layers. The Se–Se distance between the layers is 3.868 Å. The unit cell is indicated with solid blue lines.

size-selective centrifugation at various speeds. If the solvent is chosen appropriately,[19] the nanosheets will be stable against reaggregation and precipitation. This relatively inexpensive technique gained popularity for the large-scale synthesis and functionalization of 2D materials.

Driven by our interest in the synthesis of 2D magnetic materials, we have decided to apply the LPE method for the production of nanosheets of a layered magnet. Surprisingly, to the best of our knowledge, no such studies have been reported thus far. Our material of choice is $MnIn_2Se_4$, a semiconductor with potentially interesting photoelectronic properties. Its structure consists of slabs of four Se layers, between which are sandwiched Mn and In atoms (Fig. 1). These slabs are separated by van-der-Waals interactions between the Se atoms, with the minimum Se–Se distance of 3.868 Å. Although the presence of the triangular layer of Mn^{2+} ions might suggest interesting magnetic properties due to the frustrated geometric arrangement of spins,[24,25] the material only exhibits spin-glass behavior at 3.5 K attributed to antisite disorder between the Mn and In atoms.[26] Despite the somewhat unremarkable magnetic behavior, the van-der-Waals gap of this material resembles that of TMDs and, thus, suggests that $MnIn_2Se_4$ should remain air-stable in the ultrathin form. This consideration is important, because, unfortunately, the majority of 2D magnets studied to date are highly air-sensitive, which impedes their investigation.

In this work, we describe the LPE of $MnIn_2Se_4$ into few-nm thick sheets and investigate the magnetic behavior of this 2D material. We demonstrate that the spin-glass behavior is preserved in thicker sheets but lost in thinner ones. We discuss possible reasons for this observation, as well as pathways for future studies on this and related magnetic materials.

Results and discussion

Synthesis

Crystalline $MnIn_2Se_4$ was obtained by chemical vapor transport (CVT) that followed a previously reported procedure.[27] The phase purity of the sample was confirmed by powder X-ray diffraction (PXRD) that also revealed preferred orientation along the [001] direction (Fig. S1, ESI†), perpendicular to the 7-atom-thick layers observed in the crystal structure of $MnIn_2Se_4$. The unit cell refinement confirmed the trigonal lattice (space group $R\bar{3}m$) with unit cell parameters a = 4.05(1) Å and c = 39.3(4) Å, which were in agreement with the reported values of a = 4.051 Å and c = 39.464 Å.[26]

The length of the unit cell along the c axis corresponds to three 7-atom-thick slabs (Fig. 1). These layers are separated by a van-der-Waals distance of 3.868 Å between the Se atoms, suggesting that this material should be easily cleavable to produce ultrathin nanosheets. Indeed, a recent work has demonstrated a possibility of obtaining such nanosheets by mechanical exfoliation.[27]

Liquid-phase exfoliation

To prepare nanosheets of $MnIn_2Se_4$ on a larger scale, we turned to the LPE method. The bulk samples obtained by CVT were ground and exfoliated by tip ultrasonication under inert atmosphere of argon gas. This method affords faster and more efficient LPE as compared to the more common low-energy bath sonication. Prior to exfoliation, the bulk samples were soaked in water for a few minutes, as such pre-soaking has been shown to facilitate the subsequent LPE.[28] After water was decanted, the samples were slightly dried and dispersed in isopropyl alcohol (IPA), *N*-methylpyrrolidine (NMP), acetone, and some other solvents for ultrasonication (Table S1, ESI†). We found that ultrasonication in IPA produced the most stable suspensions of nanosheets. The suspensions obtained with all other solvents were unstable, with $MnIn_2Se_4$ precipitating after relatively short time (Fig. S2, ESI†). In contrast, the suspension of nanosheets exfoliated in IPA remained stable for a few weeks. Sonicating the samples for a longer time (5–7 h) improves the effectiveness of exfoliation.

The suitability of IPA for exfoliating $MnIn_2Se_4$ could be attributed to good match between the surface energies of the solvent and the layered material. Such a match allows stabilization of the exfoliated nanosheets without substantial repulsive interactions, as was demonstrated in earlier works.[19]

The size selection of the exfoliated nanosheets was achieved by using a cascade of centrifugation steps (Fig. S3, ESI†). After ultrasonication, the suspensions of nanosheets in IPA were immediately subjected to centrifugation at low speed (1000 rpm) to remove any unexfoliated material as sediment. The supernatant was collected and then centrifuged at higher speed (2000 rpm). The newly formed precipitate was separated from the supernatant, which was subjected to centrifugation at 5000 rpm, and the precipitate obtained was separated from the supernatant yet again. Finally, the remaining supernatant was centrifuged at 7500, and the new precipitate was collected.

The remaining supernatant was discarded. The precipitate obtained at each stage was labeled with the corresponding centrifugation speed and re-dispersed in a small volume of IPA (2–3 mL). These suspensions were stable for weeks, even when stored under ambient conditions. PXRD patterns of exfoliated sheets (Fig. S4, ESI†) showed that the $MnIn_2Se_4$ structure was preserved after exfoliation, although slight peak broadening was observed, which we attribute to the substantially decreased thickness of the sheets in comparison to the bulk sample.

Microscopic and spectroscopic characterization

The size-selected samples, re-dispersed in IPA, were drop-cast onto SiO_2/Si wafers and examined by scanning electron microscopy (SEM), which confirmed that the composition of all samples was close to $Mn_{0.9}In_2Se_4$ (Table S1, ESI†), suggesting the minor vacancy concentration in the Mn sites. From the SEM images (Fig. 2a–c), it is evident that the starting materials have been exfoliated successfully. The samples collected at higher centrifugation speeds, in general, contained thinner flakes, which also had smaller lateral sizes, as revealed by transmission electron microscopy (TEM) and annual dark-field scanning TEM (STEM) imaging (Fig. 2d–f). Thus, while the bulk plate-like crystals had the average lateral size of 3–5 mm, the average lateral size was ~1.5 μm and <1 μm for the sheets collected at 2000 and 7500 pm, respectively.

The samples collected at both 2000 and 5000 rpm showed substantial clustering of sheets. To allow for better imaging, the re-dispersed 5000 rpm sample was centrifuged at a lower speed (2000 rpm), and the precipitated residue was removed, while the supernatant was used for further analysis. This operation decreased clustering of the sheets, thus allowing for better SEM imaging. EDX analysis showed the elemental composition of the exfoliated materials remained intact, with the Mn : In : Se ratio consistently close to 1 : 2 : 4 (Table S1, ESI†).

To estimate the thickness of the exfoliated sheets, diluted IPA suspensions were drop-cast on Cu grids and studied by TEM with electron energy loss spectroscopy (EELS). The log-ratio EELS analysis (Fig. S5, ESI†) of individual crystal sheets revealed the average thickness of 50, 40, and 14 nm for the sheets isolated at 2000, 5000, and 7500 rpm, respectively. Clearly, the increase in the centrifugation speed allows isolation of thinner sheets. The thickness of sheets isolated at 2000 rpm corresponds approximately to 12 unit cells, or 36 7-atom-thick Mn–In–Se layers, where each heptatomic layer is ~1.3 nm thick. The sheets collected at 5000 rpm and 7500 rpm have the thickness of 30 and 10 heptatomic layers, respectively. Although we were not able to detect sheets with the thickness of one heptatomic layer, we will show below that the properties of the relatively thick sheets still change as compared to the properties of the bulk material.

Since $MnIn_2Se_4$ is a known semiconducting material, its optoelectronic properties are well documented. Earlier reports have shown a direct band gap of 1.85 eV,[29] but more recent studies found an indirect band gap at $E_g \approx 1.37$ eV.[30] We measured photoluminescence (PL) spectra of bulk $MnIn_2Se_4$ and suspensions of nanosheets isolated at 5000 rpm and 7500 rpm (it was not possible to record the spectrum of the sample collected at 2000 rpm, due to a very large scattering caused by the larger size of the sheets). The bulk sample showed a dominant PL band with the maximum at 2.90 eV and a smaller peak at 1.55 eV (Fig. 3a). The same features at 2.90 and 1.65 eV were observed in the PL spectrum of the sample collected at 5000 rpm (Fig. 3b). For the sample collected at 7500 rpm, the major PL band is still observed at 2.80 eV, but the small peak at lower energy is substantially diminished (Fig. 3c). We attribute the dominant higher-energy peak to the direct-band-gap photoemission and the weaker lower-energy peak to the indirect-band-gap transition.

To gain further insight into the origin of the PL bands, we recorded a UV-vis absorption spectrum of the sample collected at 7500 rpm (Fig. 4a), as the scattering from this sample suspended in IPA was sufficiently low to allow collection of the spectrum in the transmission mode. The Tauc plot was used to evaluate the band gap of the sample.[31] Extrapolating the linear segment of the $(\alpha h\nu)^2$ *vs.* $h\nu$ plot (where α is absorbance, h is Planck's constant, and ν is frequency) gave the value of the direct band gap equal to 3.0 eV (Fig. 4b), consistent with the energy of the major PL peak (Fig. 3c). The indirect band gap was evaluated by fitting the absorbance spectrum to the Boltzmann function[31] (Fig. S6, ESI†). The fitting procedure, described in the ESI† file, resulted in the indirect band gap of 1.8 eV, which is similar to the energy of the minor peak observed in the PL spectra (Fig. 3).

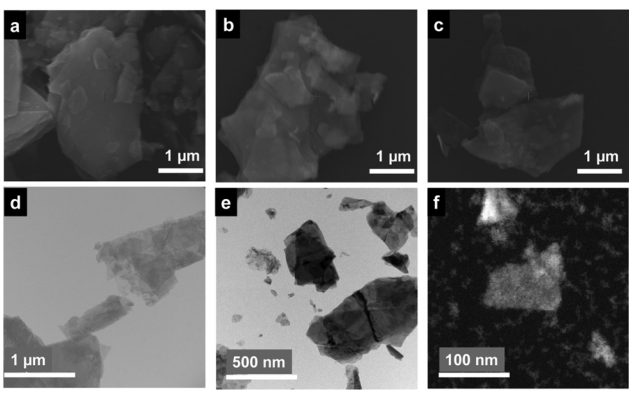

Fig. 2 SEM images of exfoliated $MnIn_2Se_4$ samples isolated at 2000 rpm (a), 5000 rpm (b), and 7500 rpm (c), respectively, and the corresponding TEM images of sheets collected at 2000 rpm (d) and 5000 rpm (e) and an annual dark-field STEM image of sheets collected at 7500 rpm (f).

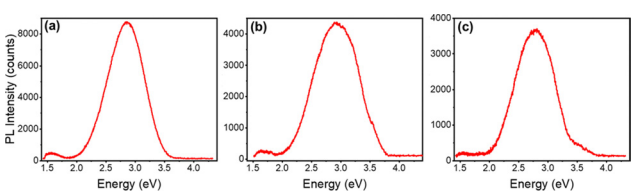

Fig. 3 Photoluminescence spectra of bulk $MnIn_2Se_4$ (a) and of sheets collected at 5000 rpm (b) and 7500 rpm (c).

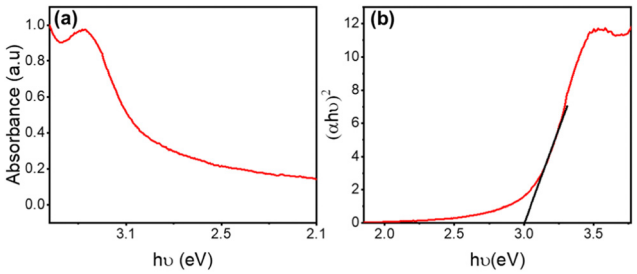

Fig. 4 (a) UV-Vis absorption spectrum of the $MnIn_2Se_4$ sheets collected at 7500 rpm. (b) The Tauc plot used to evaluate the direct band gap of the material.

Magnetic properties

Magnetic measurements performed on the bulk sample of $MnIn_2Se_4$ revealed that the temperature dependence of inverse magnetic susceptibility shows a good fit to the Curie–Weiss law, $1/\chi = (T - \theta)/C$, above 100 K (Fig. 5a). The Curie constant, C = 3.40(1) emu K mol^{-1} (μ_{eff} = 5.22 μ_B) is substantially lower than the expectation value of 4.375 emu K mol^{-1} (5.92 μ_B) for the free S = 5/2 Mn^{2+} ion. Such deviation is explained by partial quenching of the Mn magnetic moment due to the covalency of the Mn–Se bonds.[32–34] The negative Weiss constant, θ = −81.7(1) K, indicates antiferromagnetic (AFM) interactions between the Mn^{2+} ions. Despite this relatively strong exchange coupling, the material does not exhibit AFM ordering, in agreement with the previous reports.[35–39] The lack of AFM ordering is explained both by the spin frustration, due to the triangular arrangement of Mn spins, and the antisite disorder of the Mn and In atoms. The AC susceptibility measurements revealed a frequency-dependent maximum in the temperature dependence of χ' (Fig. 5b), which confirms the spin-glass state formed in the bulk material below 3 K. The Mydosh parameter (φ), calculated from the temperature dependence of χ' at different frequencies (*c.f.* ESI†), was equal to 0.028, which falls in the typical range for spin-glass materials.[40]

Magnetic measurements performed on the exfoliated samples revealed behavior similar to that of the bulk sample, without any anomalies that would suggest magnetic ordering (Fig. S7, ESI†). This observation also indicates the lack of any magnetic oxide impurities that could form due to surface

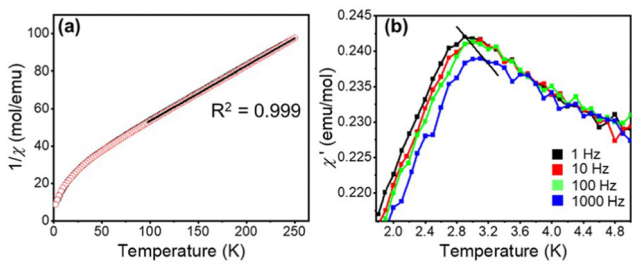

Fig. 5 The temperature dependence of inverse DC magnetic susceptibility (a) and of in-phase AC susceptibility (b) for the bulk sample of $MnIn_2Se_4$. The Curie–Weiss fit is shown with a solid black line in panel (a), while the black line in panel (b) is used to emphasize the frequency-dependent maximum characteristic of the spin-glass state.

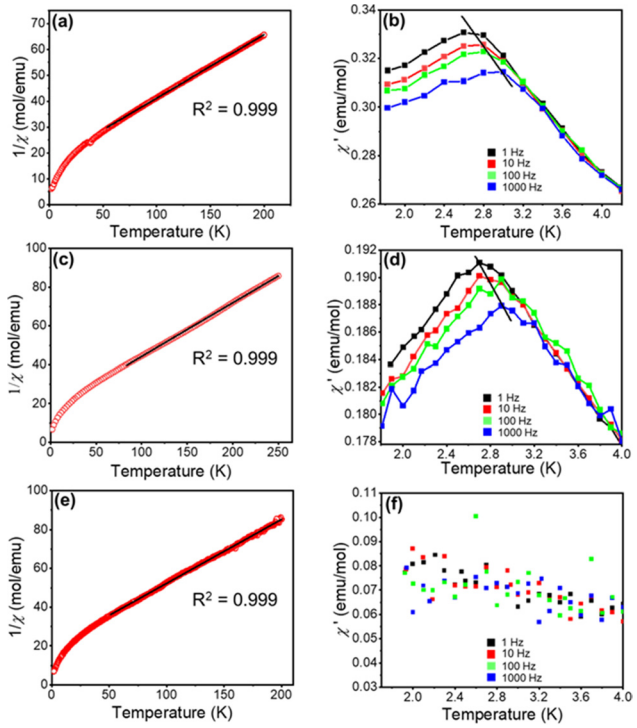

Fig. 6 The temperature dependence of inverse DC magnetic susceptibility (left) and of in-phase AC magnetic susceptibility (right) for the sheets isolated at 2000 rpm (a and b), 5000 rpm (c and d), and 7500 rpm (e and f). The Curie–Weiss fits are shown with solid black lines in panels (a), (c), and (e), while in panels (b) and (d) the lines are used to emphasize the frequency-dependent maxima characteristic of the spin-glass state.

oxidation (*e.g.*, MnO shows AFM ordering at 118 K[41] and Mn_3O_4 shows ferrimagnetic ordering at 42 K[42]). We note that such oxidation is unlikely, since the samples were exfoliated under Ar atmosphere and the sheets are likely to be covered abundantly with surfactant IPA and water molecules. Indeed, XPS measurements on the sheets isolated at 2000 rpm showed dominant signals from C and O atoms, in ∼2 : 1 ratio (Fig. S8, ESI†).

The Curie–Weiss fit of the $1/\chi$ *vs.* T curves measured for the exfoliated samples (Fig. 6a, c, and e) gave the C and θ parameters on the same order of magnitude as those observed for the bulk material (Table 1). The AC susceptibility for the samples isolated at 2000 and 5000 rpm also showed a frequency-dependent peak in the temperature dependence of χ'. The presence of this feature, together with the calculated Mydosh parameter of 0.034 and 0.014, respectively, confirms

Table 1 The summary of magnetic parameters determined for the bulk $MnIn_2Se_4$ and for the thin sheets isolated at different centrifugation speeds. The last column provides the values of the Mydosh parameter (see the ESI for details)

$MnIn_2Se_4$ Sample	C (emu K mol^{-1})	μ_{eff} (μ_B)	θ (K)	φ
Bulk	3.40(1)	5.22	−81.7(1)	0.028
2000 rpm	3.14(8)	5.01	−68.52(5)	0.034
5000 rpm	3.64(3)	5.40	−61.55(8)	0.014
7500 rpm	3.02(1)	4.90	−58.3(9)	—

the spin-glass behavior of the exfoliated samples, similar to the bulk sample of $MnIn_2Se_4$. The temperature of the cusp in the χ' *vs.* T plot decreased by ~0.2–0.3 K in the exfoliated sheets as compared to the bulk sample (Table S2, ESI†), indicating slightly lower spin-glass transition temperatures for the nanosheets. Interestingly, we did not observe any feature in the AC susceptibility measurements of the sample isolated at 7500 rpm. A possible reason is the small amount of the sample that was isolated, which could decrease the AC signal below the detection limit of the instrument. It is also possible that the spin-glass freezing temperature was shifted below 1.8 K, due to the flakes isolated in the last centrifugation step being substantially thinner.

Yang *et al.*[27] reported mechanical exfoliation of $MnIn_2Se_4$, down to the thickness of 3 heptatomic layers (one unit cell along the *c* axis). They suggested that the 2D sample of $MnIn_2Se_4$ undergoes a ferromagnetic transition at 7 K. Their claim, however, is questionable, since the temperature dependence of magnetization presented in that work appears to be more consistent with the spin-glass behavior. Unfortunately, the authors did not perform additional AC measurements to confirm or disproof the long-range magnetic ordering. In our opinion, the question remains open, but our present results strongly suggest that the decrease in the thickness of $MnIn_2Se_4$ does not lead to the change in the type of magnetic exchange.

Conclusions

This work demonstrates liquid-phase exfoliation of relatively thin sheets of the layered $MnIn_2Se_4$ structure, which is built of heptatomic layers terminated by Se atoms. Isopropanol offers effective medium for both exfoliation of the bulk material and re-dispersion of the exfoliated sheets. The thinnest sheets observed by TEM/EELS measurements were 14 nm thick. Exfoliation to even thinner sheets might be possible, but the decrease in the amount of material remaining after sequential centrifugation steps at increasing speeds did not allow to observe thinner 2D structures. Current efforts in our labs focus on scaling up the exfoliation protocols and applying them to other semiconducting and magnetic van-der-Waals materials with layers thicker than 3 atoms.

Experimental

Starting materials

Powders of Mn (99.98%, Alfa Aesar), In (99.999%, VWR), and Se (99.999%, VWR) were used as received. 2-Propanol (isopropyl alcohol, IPA) was purchased from Sigma-Aldrich and also used as received.

Synthesis

Crystal of $MnIn_2Se_4$ were grown by CVT, following a procedure reported earlier.[27] Powders of Mn, In, and Se were combined in a stoichiometric ratio (the total mass = 0.5 g) in an Ar-filled dry box (content of O_2 < 0.1 ppm) and loaded in a fused silica tube with the inner diameter of 10 mm. The tube was taken out of the box, 30 mg of I_2 as transport agent was quickly added, and the tube was sealed under vacuum (~10^{-4} mbar). The 20 cm long tube was placed in a temperature gradient furnace, with the starting materials maintained at 900 °C and the sink zone held at 850 °C (the furnace was ramped to the desired temperature over 12 h). After 10 days, the temperature of the hot zone was lowered to 500 °C in 2 days, with the simultaneous decrease in the temperature of the sink, and the temperature was maintained for 1 day before cooling down to room temperature in 24 h. Large black plate-like crystals of $MnIn_2Se_4$ were collected from the sink zone of the tube. The identity of the crystals was confirmed by unit-cell determination from single-crystal X-ray diffraction.

Liquid-phase exfoliation

The crystals of $MnIn_2Se_4$ (~0.3 g) were lightly grounded with mortar and pestle. The sample obtained was stirred in water for 10 min and dried under vacuum for 24 h. The powder was dispersed in IPA, at the concentration of ~3 g L^{-1}. The dispersion was subjected to ultra-sonication for 1 h under ice-cooling in a glass vial, using a tip-sonicator (QSONICA) at 60% amplitude. To prevent sample oxidation, all ultra-sonication procedures were carried out under Ar atmosphere. The resultant dispersion was centrifuged at 5000 rpm for 1.5 h to remove any low-quality material or minor impurities.[19] The supernatant was discarded, and the precipitate was redispersed in fresh IPA and subjected to longer sonication for 7 h at 60% amplitude (with 6 s/2 s on/off pulsing), after which the dispersion was subjected to centrifugation at 1000 rpm for 60 min to remove larger particles. The sediment was discarded, and the supernatant was subjected to a series of size-selective centrifugation steps performed at sequentially increasing rotation speeds of 2000, 5000, and 7500 rpm. At each step, the precipitate isolated by 45–60 min long centrifugation was separated, re-dispersed in 2–3 mL of fresh IPA, and stored for further characterization, while the supernatant was subjected to the next centrifugation step. The centrifugation was carried out at low temperature (15 °C) to prevent re-aggregation of the nanosheets due to heating.

Physical measurements

PXRD data were collected at room temperature using Panalytical X'Pert Pro X-ray diffractometer with an X'Celerator detector and a Cu-Kα source (λ = 1.54187 Å). The patterns were recorded in the 2θ range from 10° to 80° with a step of 0.05° and the total collection time of 1 h. The data analysis was performed with Highscore Plus.[43] Elemental analysis of the exfoliated sheets was performed on a JEOL 5900 scanning electron microscope with an energy-dispersive (EDX) microanalysis attachment. Magnetic properties were measured on polycrystalline bulk samples and exfoliated sheets using a magnetic property measurement system MPMS-XL (Quantum Design) equipped with a superconducting quantum interference device (SQUID). Field-cooled (FC) and zero-field-cooled (ZFC) magnetization measurements were carried out in the temperature range of 1.8–250 K in a

direct-current applied field of 100 Oe. Alternating-current (AC) susceptibility was measured in the 1.8–5 K temperature range, with the AC field amplitude of 5 Oe at frequencies of 1, 10, 100, and 1000 Hz.

Author contributions

G. Sasi Kumar: methodology, investigation, formal analysis, validation, visualizatoin, writing – original draft. Y. Xin: investigation, formal analysis, visualization, writing – review & editing. J. S. R. Vellore Winfred: investigation, validation. J. K. Clark: methodology, investigation, writing – review & editing. M. Shatruk: conceptualization, methodology, formal analysis, visualization, funding acquisition, supervision, writing – review & editing.

Conflicts of interest

There are no conflicts to declare.

Acknowledgements

This research was supported by the National Science Foundation (NSF, award DMR-1905499). TEM work was performed at National High Magnetic Field Laboratory supported by NSF Cooperative Agreement DMR-1644779 and the State of Florida. The project also used resources provided by the X-ray Crystallography Center (FSU075000XRAY) and the Materials Characterization Laboratory (FSU075000MAC) at the Department of Chemistry and Biochemistry, Florida State University. We would like to acknowledge Dr Eric Lochner with assistance in collecting and interpreting the XPS data.

Notes and references

1 R. Mas-Ballesté, C. Gómez-Navarro, J. Gómez-Herrero and F. Zamora, 2D materials: to graphene and beyond, *Nanoscale*, 2011, **3**, 20–30.
2 K. S. Novoselov, A. Mishchenko, A. Carvalho and A. H. Castro, Neto, 2D materials and van der Waals heterostructures, *Science*, 2016, **353**, aac9439.
3 C. L. Tan, X. H. Cao, X. J. Wu, Q. Y. He, J. Yang, X. Zhang, J. Z. Chen, W. Zhao, S. K. Han, G. H. Nam, M. Sindoro and H. Zhang, Recent advances in ultrathin two-dimensional nanomaterials, *Chem. Rev.*, 2017, **117**, 6225–6331.
4 N. R. Glavin, R. Rao, V. Varshney, E. Bianco, A. Apte, A. Roy, E. Ringe and P. M. Ajayan, 2D Materials: emerging applications of elemental 2D materials, *Adv. Mater.*, 2020, **32**, 2070052.
5 Q. Ma, G. Ren, K. Xu and J. Z. Ou, Tunable optical properties of 2D materials and their applications, *Adv. Opt. Mater.*, 2021, **9**, 2001313.
6 Z. Wu and J. Hao, Electrical transport properties in group-V elemental ultrathin 2D layers, *npj 2D Mater. Appl.*, 2020, **4**, 4.
7 K. F. Mak, J. Shan and D. C. Ralph, Probing and controlling magnetic states in 2D layered magnetic materials, *Nat. Rev. Phys.*, 2019, **1**, 646–661.
8 T. A. Shifa, F. Wang, Y. Liu and J. He, Heterostructures based on 2D materials: a versatile platform for efficient catalysis, *Adv. Mater.*, 2019, **31**, 1804828.
9 R. Worsley, L. Pimpolari, D. McManus, N. Ge, R. Ionescu, J. A. Wittkopf, A. Alieva, G. Basso, M. Macucci, G. Iannaccone, K. S. Novoselov, H. Holder, G. Fiori and C. Casiraghi, All-2D material inkjet-printed capacitors: toward fully printed integrated circuits, *ACS Nano*, 2019, **13**, 54–60.
10 D. Wang, X.-B. Li and H.-B. Sun, Modulation doping: a strategy for 2D materials electronics, *Nano Lett.*, 2021, **21**, 6298–6303.
11 X. Liu and M. C. Hersam, 2D materials for quantum information science, *Nat. Rev. Mater.*, 2019, **4**, 669–684.
12 H. Huang, Y. Xu, J. Wang and W. Duan, Emerging topological states in quasi-two-dimensional materials, *Wiley Interdiscip. Rev.: Comput. Mol. Sci.*, 2017, **7**, e1296.
13 D. Qiu, C. Gong, S. Wang, M. Zhang, C. Yang, X. Wang and J. Xiong, Recent advances in 2D superconductors, *Adv. Mater.*, 2021, **33**, 2006124.
14 B. Huang, G. Clark, E. Navarro-Moratalla, D. R. Klein, R. Cheng, K. L. Seyler, D. Zhong, E. Schmidgall, M. A. McGuire, D. H. Cobden, W. Yao, D. Xiao, P. Jarillo-Herrero and X. Xu, Layer-dependent ferromagnetism in a van der Waals crystal down to the monolayer limit, *Nature*, 2017, **546**, 270–273.
15 C. Gong, L. Li, Z. Li, H. Ji, A. Stern, Y. Xia, T. Cao, W. Bao, C. Wang, Y. Wang, Z. Q. Qiu, R. J. Cava, S. G. Louie, J. Xia and X. Zhang, Discovery of intrinsic ferromagnetism in two-dimensional van der Waals crystals, *Nature*, 2017, **546**, 265–269.
16 J. Yu, J. Li, W. Zhang and H. Chang, Synthesis of high quality two-dimensional materials via chemical vapor deposition, *Chem. Sci.*, 2015, **6**, 6705–6716.
17 Z. Li, R. J. Young, C. Backes, W. Zhao, X. Zhang, A. A. Zhukov, E. Tillotson, A. P. Conlan, F. Ding, S. J. Haigh, K. S. Novoselov and J. N. Coleman, Mechanisms of liquid-phase exfoliation for the production of graphene, *ACS Nano*, 2020, **14**, 10976–10985.
18 C. Huo, Z. Yan, X. Song and H. Zeng, 2D materials via liquid exfoliation: a review on fabrication and applications, *Sci. Bull.*, 2015, **60**, 1994–2008.
19 C. Backes, T. M. Higgins, A. Kelly, C. Boland, A. Harvey, D. Hanlon and J. N. Coleman, Guidelines for exfoliation, characterization and processing of layered materials produced by liquid exfoliation, *Chem. Mater.*, 2017, **29**, 243–255.
20 J. N. Coleman, Liquid exfoliation of defect-free graphene, *Acc. Chem. Res.*, 2013, **46**, 14–22.
21 L. Li, M. Zhou, L. Jin, L. Liu, Y. Mo, X. Li, Z. Mo, Z. Liu, S. You and H. Zhu, Research progress of the liquid-phase exfoliation and stable dispersion mechanism and method of graphene, *Front. Mater.*, 2019, **6**, 325.
22 B. Adilbekova, Y. Lin, E. Yengel, H. Faber, G. Harrison, Y. Firdaus, A. El-Labban, D. H. Anjum, V. Tung and T. D. Anthopoulos, Liquid phase exfoliation of MoS_2 and WS_2 in aqueous ammonia and their application in highly efficient organic solar cells, *J. Mater. Chem. C*, 2020, **8**, 5259–5264.

23 B. Zhang, Q. Wu, H. Yu, C. Bulin, H. Sun, R. Li, X. Ge and R. Xing, High-efficient liquid exfoliation of boron nitride nanosheets using aqueous solution of alkanolamine, *Nanoscale Res. Lett.*, 2017, **12**, 596.

24 A. P. Ramirez, Strongly geometrically frustrated magnets, *Annu. Rev. Mater. Sci.*, 1994, **24**, 453–480.

25 L. Balents, Spin liquids in frustrated magnets, *Nature*, 2010, **464**, 199–208.

26 K. J. Range, U. Klement, G. Döll, E. Bucher and J. R. Baumann, The crystal structure of $MnIn_2Se_4$, a ternary layered semiconductor, *Z. Naturforsch. B*, 1991, **46**, 1122–1124.

27 J. Yang, Z. Zhou, J. Fang, H. Wen, Z. Lou, G. Shen and Z. Wei, Magnetic and transport properties of a ferromagnetic layered semiconductor $MnIn_2Se_4$, *Appl. Phys. Lett.*, 2019, **115**, 222101.

28 F. I. Alzakia, W. Jonhson, J. Ding and S. C. Tan, Ultrafast exfoliation of 2D materials by solvent activation and one-step fabrication of all-2D-material photodetectors by electrohydrodynamic printing, *ACS Appl. Mater. Interfaces*, 2020, **12**, 28840–28851.

29 C. Rincón, T. E. Torrres, V. Sagredo, S. J. Jiménez-Sandoval and E. Mares-Jacinto, The fundamental absorption edge in $MnIn_2Se_4$ layer semi-magnetic semiconductor, *Physica B*, 2015, **477**, 123–128.

30 H. Neumann, C. Bellabarba, A. Khan and V. Riede, Optical Properties of $MnIn_2Se_4$, *Cryst. Res. Technol.*, 1986, **21**, K21–K24.

31 A. R. Zanatta, Revisiting the optical bandgap of semiconductors and the proposal of a unified methodology to its determination, *Sci. Rep.*, 2019, **9**, 11225.

32 J. K. Clark, V. Yannello, A. M. Samarakoon, C. Ross, M. C. Uible, V. O. Garlea and M. Shatruk, Inelastic neutron scattering study of magnetic exchange pathways in MnS, *J. Phys. Chem. C*, 2021, **125**, 16183–16190.

33 J. K. Clark, C. Pak, H. Cao and M. Shatruk, Helimagnetism in $MnBi_2Se_4$ driven by spin-frustrating interactions between antiferromagnetic chains, *Crystals*, 2021, **11**, 242.

34 A. Bhutani, P. Behera, R. D. McAuliffe, H. Cao, A. Huq, M. J. Kirkham, C. R. dela Cruz, T. Woods and D. P. Shoemaker, Incommensurate magnetism in $K_2MnS_{2-x}Se_x$ and prospects for tunable frustration in a triangular lattice of pseudo-1D spin chains, *Phys. Rev. Mater.*, 2019, **3**, 064404.

35 G. Döll, A. Anghel, J. R. Baumann, E. Bucher, A. P. Ramirez and K. J. Range, Structural and magnetic properties of the ternary manganese compound semiconductors $MnAl_2Te_4$, $MnIn_2Te_4$, and $MnIn_2Se_4$, *Phys. Status Solidi A*, 1991, **126**, 237–244.

36 M. Quintero, M. Morocoima, A. Rivero, P. Bocaranda and J. C. Woolley, $Cu_{2(1-z)}Mn_zln_2Se_4$ alloys; phase diagram and effects of Mn ordering on magnetic behaviour, *J. Phys. Chem. Solids*, 1997, **58**, 491–496.

37 R. Tovar, M. Quintero, E. Quintero, P. Bocaranda, J. Ruiz, A. E. Mora, L. Höeger and J. M. Briceño, Magnetic behaviour for the $MnIn_{2(1-z)}Ga_{2z}Se_4$ alloys, *Phys. Status Solidi B*, 2000, **220**, 435–439.

38 J. C. M. Ochoa, V. Bindilatti, E. ter Haar, J. A. H. Coaquira, G. E. de Souza Brito, X. Gratens and V. Sagredo, Spin glass behavior in $MnIn_2Se_4$ and $Zn_{1-x}Mn_xIn_2Se_4$ magnetic semiconductors, *J. Magn. Magn. Mater.*, 2004, **272–276**, 1308–1309.

39 J. Mantilla, E. Ter Haar, J. A. H. Coaquira and V. Bindilatti, Experimental evidence of the spin-glass transition in the diluted magnetic semiconductor $Zn_{1-x}Mn_xIn_2Se_4$, *J. Phys.: Condens. Matter*, 2008, **20**, 455211.

40 J. A. Mydosh, *Spin glasses: an experimental introduction*, Taylor & Francis, Washington, DC, 1993.

41 C. F. Squire, Antiferromagnetism in some manganous compounds, *Phys. Rev.*, 1939, **56**, 922–925.

42 W. S. Seo, H. H. Jo, K. Lee, B. Kim, S. J. Oh and J. T. Park, Size-dependent magnetic properties of colloidal Mn3O4 and MnO nanoparticles, *Angew. Chem., Int. Ed.*, 2004, **43**, 1115–1117.

43 PANalytical B.V., Almelo, Netherlands, 2006.